OPEN ACCESS Freely available online

PLOS ONE

Numerical and Series Solutions for Stagnation-Point Flow of Nanofluid over an Exponentially Stretching Sheet

Meraj Mustafa[1]*, Muhammad A. Farooq[2], Tasawar Hayat[3,4], Ahmed Alsaedi[4]

1 Research Centre for Modeling and Simulation, National University of Sciences and Technology, Islamabad, Pakistan, **2** Centre for Advanced Mathematics and Physics, National University of Sciences and Technology, Islamabad, Pakistan, **3** Department of Mathematics, Quaid-I-Azam University, Islamabad, Pakistan, **4** Department of Mathematics, Faculty of Science, King Abdulaziz University, Jeddah, Saudi Arabia

Abstract

This investigation is concerned with the stagnation-point flow of nanofluid past an exponentially stretching sheet. The presence of Brownian motion and thermophoretic effects yields a coupled nonlinear boundary-value problem (BVP). Similarity transformations are invoked to reduce the partial differential equations into ordinary ones. Local similarity solutions are obtained by homotopy analysis method (HAM), which enables us to investigate the effects of parameters at a fixed location above the sheet. The numerical solutions are also derived using the built-in solver bvp4c of the software MATLAB. The results indicate that temperature and the thermal boundary layer thickness appreciably increase when the Brownian motion and thermophoresis effects are strengthened. Moreover the nanoparticles volume fraction is found to increase when the thermophoretic effect intensifies.

Citation: Mustafa M, Farooq MA, Hayat T, Alsaedi A (2013) Numerical and Series Solutions for Stagnation-Point Flow of Nanofluid over an Exponentially Stretching Sheet. PLoS ONE 8(5): e61859. doi:10.1371/journal.pone.0061859

Editor: Jeongmin Hong, University of California, Berkeley, United States of America

Received December 7, 2012; **Accepted** March 15, 2013; **Published** May 9, 2013

Funding: The paper was funded by the Deanship of Scientific Research, King Abdulaziz University (KAU), under grant no. (10-130/1433 Hi Ci). The authors, therefore, acknowledge the technical and financial support of KAU. The support is in the form of project for academic research at KAU. This is to certify that this work is not funded through any external source/research organization including industry etc. The funders had no role in study design, data collection and analysis, decision to publish, or preparation of the manuscript.

Competing Interests: The authors have declared that no competing interests exist.

* E-mail: meraj_mm@hotmail.com

Introduction

There has been great interest of researchers in the flow and heat transfer characteristics due to the impulsive motion of stretching sheet. A variety of technical processes involve the production of sheeting material which includes both metal and polymer sheets. The rate of heat transfer at the sheet is largely dependent on the quality of final product.

Flow past a flat plate with a uniform free stream was reported by Blasius [1]. In contrast to the Blasius problem, the boundary layer flow over a continuously moving plate in a quiescent ambient fluid was explored by Sakiadis [2]. Crane [3] extended this concept for a sheet which is stretched with the velocity linearly proportional to the distance from the origin. Since this pioneering work of Crane [3], the literature concerning the boundary layer flows past a stretching sheet has been in continuous growing. In fact Crane's problem has been considered for several other features such as viscoelasticity, heat and mass transfer, porosity, magnetic field etc. (see Rajagopal et al. [4], Mahapatra and Gupta [5], Cortell [6], Bachok et al. [7], Abbasbandy and Ghehsareh [8], Fang et al. [9], Hayat et al. [10], Mustafa et al. [11,12] etc.). On the other hand, a literature survey witnesses that the flow analysis over an exponentially stretching sheet has been scarcely presented. Combined heat and mass transfer in the boundary layer flow over an exponentially stretching sheet has been reported by Magyari and Keller [13]. Suction and heat transfer characteristics in the exponentially stretched flow has been studied by Elbashbeshy [14]. Viscoelastic effects in the flow over an exponentially stretching sheet have been described by Khan and Sanjayanand [15]. Analytic solutions for flow and heat transfer over an exponentially stretching sheet have been provided by Sajid and Hayat [16]. Nadeem et al. [17] examined the flow and heat transfer of viscoelastic (second grade) fluid over an exponentially sheet in the presence of thermal radiation.

Nanofluid is a liquid suspended with nanometer-sized particles (diameter less than 50 nm) called nanoparticles. These nanoparticles are typically made of metals, oxides and carbides or carbon nanotubes. In the past, the concept of nanofluids has been used as a route to enhance the performance of heat transfer rate in liquids. Detailed review studies on nanofluids have been conducted by Daungthongsuk and Wongwises [18], Wang and Mujumdar [19,20] and Kakaç and Pramuanjaroenkij [21]. Natural convective boundary layer flow of nanofluid past a vertical flat plate has been studied by Kuznetsov and Nield [22]. The Cheng-Mincowcz problem for flow of nanofluid embedded in a porous medium has been considered by Nield and Kuznetsov [23]. Bachok et al. [24] examined the flow of nanofluid over a continuously moving surface with a parallel free stream. Flow of nanofluid over a linearly stretching sheet has been studied by Khan and Pop [25]. Finite element analysis for flow of nanofluid over a nonlinearly stretching sheet is presented by Rana and Bhargava [26]. Falkner-skan problem for flow of nanofluid with with prescribed surface heat flux is investigated by Yacob et al. [27]. Makinde and Aziz [28] discussed the effect of convective boundary conditions on the

flow of nanofluid over a stretching sheet. Analytic solutions for stagnation-point flow of nanofluid over a linearly stretching sheet are obtained by Mustafa et al. [29].

It is noticed that flow of nanofluid over an exponentially stretching sheet is never reported in the literature. Thus current work presents a theoretical study on the stagnation-point flow of nanofluid over an exponentially stretching sheet. The series expressions of velocity, temperature and nanoparticles concentration are developed by homotopy analysis method (HAM) developed by Liao [30]. This method is successfully applied to derive analytic solutions of variety of nonlinear problems [30–35]. The numerical solutions are obtained by the software MATLAB. Graphical results for various values of the parameters are presented to gain thorough insight towards the physics of the problem. The numerical values of reduced Nusselt number and reduced Sherwood number for different values of the parameters are also tabulated.

Mathematical Formulation

We investigate the laminar boundary layer flow of a nanofluid in the region of stagnation-point towards an exponentially stretching sheet situated at $y=0$. The $x-$ and $y-$ axis are taken along and perpendicular to the sheet and the flow is confined to $y\geq 0$. The effects of Brownian motion and thermophoresis are also accounted. $U_w(x)=a\exp(x/l)$ denotes the velocity of the sheet while the velocity of the external flow is $U_\infty(x)=b\exp(x/l)$. Let $T_w=T_\infty+c\exp(x/l)$ and $C_w=C_\infty+d\exp(x/l)$ be the temperature and nanoparticles concentration at the sheet where T_∞ and C_∞ denote the ambient temperature and concentration respectively. The boundary layer equations governing the conservation of mass, momentum, energy and nanoparticles volume fraction are (see Kuznetsov and Nield [22], Nield and Kuznetsov [23], Bachok et al. [24], Khan and Pop [25], Rana and Bhargava [26], Yacob et al. [27], Makinde and Aziz [28] and Mustafa et al. [29])

$$\frac{\partial u}{\partial x}+\frac{\partial v}{\partial y}=0, \tag{1}$$

$$u\frac{\partial u}{\partial x}+v\frac{\partial u}{\partial y}=U_\infty\frac{dU_\infty}{dx}+\nu_f\frac{\partial^2 u}{\partial y^2}, \tag{2}$$

$$u\frac{\partial T}{\partial x}+v\frac{\partial T}{\partial y}=\alpha\frac{\partial^2 T}{\partial y^2}+\tau\left[D_B\frac{\partial C}{\partial y}\frac{\partial T}{\partial y}+\frac{D_T}{T_\infty}\left(\frac{\partial T}{\partial y}\right)^2\right], \tag{4}$$

$$u\frac{\partial C}{\partial x}+v\frac{\partial C}{\partial y}=D_B\frac{\partial^2 C}{\partial y^2}+\frac{D_T}{T_\infty}\frac{\partial^2 T}{\partial y^2}. \tag{5}$$

With the boundary conditions

$$\begin{aligned}&u=U_w(x)=ae^{x/L},\ v=0,\ T=T_w(x),\ C=C_w(x)\text{ at }y=0,\\&u\to U_e(x)=be^{x/L},\quad T\to T_\infty,\ C\to C_\infty\text{ as }y\to\infty.\end{aligned} \tag{6}$$

Where u and v are the velocity components along x- and y-directions respectively, ν_f is the kinematic viscosity, α is the thermal diffusivity, D_B is the Brownian motion coefficient, D_T is the thermophoretic diffusion coefficient and $\tau(=(\rho c)_p/(\rho c)_f)$ is the ratio of effective heat capacity of the nanoparticle material to heat capacity of the fluid.

We introduce

$$\begin{aligned}&\eta=\sqrt{\frac{a}{2\nu_f L}}e^{x/2L}y,u=ae^{x/L}f'(\eta),v=-\sqrt{\frac{\nu_f a}{2L}}e^{x/2L}[f(\eta)+\eta f'(\eta)],\\&\theta(\eta)=\frac{T-T_\infty}{T_w-T_\infty},\phi(\eta)=\frac{C-C_\infty}{C_w-C_\infty},\end{aligned} \tag{7}$$

Inserting Eq. (7) into Eqs. (2)–(5) yield the following ordinary differential equations

$$f'''+ff''-2f'^2+2\lambda^2=0, \tag{8}$$

$$\frac{1}{\Pr}\theta''+f\theta'-2f'\theta+Nb\theta'\phi'+Nt\theta'^2=0, \tag{9}$$

$$\phi''+Le(f\phi'-2f'\phi)+\frac{Nt}{Nb}\theta''=0, \tag{10}$$

$$\begin{aligned}&f(0)=0,f'(0)=1,\theta(0)=1,\phi(0)=1,\\&f'(\infty)\to\lambda,\theta(\infty)\to0,\phi(\infty)\to0.\end{aligned} \tag{11}$$

$$\begin{aligned}&\lambda=\frac{b}{a},\Pr=\frac{\nu_f}{\alpha},Le=\frac{\nu_f}{D_B},\\&Nb=\frac{(\rho c)_p D_B(C_w-C_\infty)}{(\rho c)_f\nu_f},Nt=\frac{(\rho c)_p D_T(T_f-T_\infty)}{(\rho c)_f T_\infty\nu_f}.\end{aligned} \tag{12}$$

Here λ is the velocity ratio, Pr is the Prandtl number, Le is the Lewis number, Nb is the Brownian motion parameter and Nt is the thermophoresis parameter. It is clear that $x-$coordinate can not be eliminated from Eqs. (9) and (10) because Nb and Nt are functions of x. Thus we look for the availability of local similarity solutions which permits us to investigate the behaviors of these parameters at a fixed location above the sheet. $Nb=0$ corresponds to the case when there is no thermal transport generated by the nanoparticles concentration gradients.

The skin friction coefficient C_f, the local Nusselt number Nu and the local Sherwood number Sh are given by

$$C_f=\frac{\mu\left(\frac{\partial u}{\partial y}\right)_{y=0}}{\rho U_w^2},Nu=-\frac{x\left(\frac{\partial T}{\partial y}\right)_{y=0}}{(T_w-T_\infty)},Sh=-\frac{x\left(\frac{\partial C}{\partial y}\right)_{y=0}}{(C_w-C_\infty)}, \tag{13}$$

Using (7) in (13) one obtains

$$\begin{aligned}&\sqrt{2Re}C_f=f''(0),\sqrt{\frac{2L}{x}}Nu/Re_x^{1/2}=-\theta'(0)=Nur,\\&\sqrt{\frac{2L}{x}}Sh/Re_x^{1/2}=-\vartheta'(0)=Shr.\end{aligned} \tag{14}$$

where $Re=U_wL/\nu_f$ is the Reynolds number and $Re_x=U_wx/\nu_f$ denotes the local Reynolds number.

Methods of Solution

3.1 Homotopy analytic solution

Rule of solution expression and the involved boundary conditions direct us to choose the following initial guesses f_0, θ_0 and ϕ_0 of $f(\eta)$,$\theta(\eta)$ and $\phi(\eta)$

$$f_0(\eta)=\lambda\eta+(1-\lambda)(1-\exp(-\eta)),\quad \theta_0(\eta)=\phi_0(\eta)=\exp(-\eta), \tag{15}$$

The auxiliary linear operators are chosen as

$$\mathcal{L}_f\equiv\frac{d^3}{d\eta^3}-\frac{d}{d\eta},\quad \mathcal{L}_\theta\equiv\frac{d^2}{d\eta^2}-1,\quad \mathcal{L}_\phi(\phi)\equiv\frac{d^2}{d\eta^2}-1. \tag{16}$$

If $q\in[0,1]$ denotes the embedding parameter and $\hbar$ is the non-zero auxiliary parameter then the generalized homotopic equations are constructed as follows:

$$(1-q)\mathcal{L}_f[F(\eta,q)-f_0(\eta)]=q\hbar\mathcal{N}_f[F(\eta,q)], \tag{17}$$

$$(1-q)\mathcal{L}_\theta[\Theta(\eta,q)-\theta_0(\eta)]=q\hbar\mathcal{N}_\theta[F(\eta,q),\Theta(\eta,q),\Phi(\eta,q)], \tag{18}$$

$$(1-q)\mathcal{L}_\phi[\Phi(\eta,q)-\phi_0(\eta)]=q\hbar\mathcal{N}_\phi[F(\eta,q),\Theta(\eta,q),\Phi(\eta,q)], \tag{19}$$

$$F(\eta;q)|_{\eta=0}=0,\left.\frac{\partial F(\eta;q)}{\partial\eta}\right|_{\eta=0}=1,\left.\frac{\partial F(\eta;q)}{\partial\eta}\right|_{\eta\to\infty}=0, \tag{20}$$

$$\Theta(\eta;q)|_{\eta=0}=1,\Theta(\eta;q)|_{\eta\to\infty}=0, \tag{21}$$

$$\Phi(\eta;q)|_{\eta=0}=1,\Phi(\eta;q)|_{\eta\to\infty}=0, \tag{22}$$

in which the non-linear operators $\mathcal{N}_f$, $\mathcal{N}_\theta$ and $\mathcal{N}_\phi$ are

$$\begin{aligned}\mathcal{N}_f[F(\eta;q)]=&\frac{\partial^3F(\eta;q)}{\partial\eta^3}+\\ &F(\eta;q)\frac{\partial^2F(\eta;q)}{\partial\eta^2}-2\left(\frac{\partial F(\eta;q)}{\partial\eta}\right)^2+2\lambda^2,\end{aligned} \tag{23}$$

$$\begin{aligned}\mathcal{N}_\theta[F(\eta;q),\Theta(\eta;q),\Phi(\eta;q)]=&\frac{1}{\Pr}\frac{\partial^2\Theta(\eta,q)}{\partial\eta^2}+\\ &F(\eta,p)\frac{\partial\Theta(\eta,q)}{\partial\eta}-2\Theta(\eta,q)\frac{\partial F(\eta,q)}{\partial\eta}\\ &+Nb\frac{\partial\Theta(\eta,q)}{\partial\eta}\frac{\partial\Phi(\eta,q)}{\partial\eta}+Nt\left(\frac{\partial\Theta(\eta,q)}{\partial\eta}\right)^2,\end{aligned} \tag{24}$$

$$\begin{aligned}\mathcal{N}_\vartheta[F(\eta;q),\Theta(\eta;q),\Phi(\eta;q)]=&\frac{\partial^2\Phi(\eta;q)}{\partial\eta^2}+\\ &Le\left(F(\eta,q)\frac{\partial\Phi(\eta;q)}{\partial\eta}-2\Phi(\eta,q)\frac{\partial F(\eta;q)}{\partial\eta}\right)\\ &+\frac{Nt}{Nb}\frac{\partial^2\Phi(\eta,q)}{\partial\eta^2}.\end{aligned} \tag{25}$$

Using Maclaurin's series about q

$$F(\eta;q)=\sum_{m=0}^{\infty}f_m(\eta)q^m;f_m(\eta)=\frac{1}{m!}\left.\frac{\partial^mF(\eta;q)}{\partial q^m}\right|_{q=0}, \tag{26}$$

$$\Theta(\eta;q)=\sum_{m=0}^{\infty}\theta_m(\eta)q^m;\theta_m(\eta)=\frac{1}{m!}\left.\frac{\partial^m\theta(\eta;q)}{\partial q^m}\right|_{q=0}, \tag{27}$$

$$\Phi(\eta;q)=\sum_{m=0}^{\infty}\phi_m(\eta)q^m;\phi_m(\eta)=\frac{1}{m!}\left.\frac{\partial^m\phi(\eta;q)}{\partial q^m}\right|_{q=0}, \tag{28}$$

the final solutions are retrieved at $q=1$. The functions f_m,θ_m and ϕ_m can be obtained from the deformation of Eqs. (17)–(22). Explicitly the deformation problems corresponding to Eqs. (17)–(22) are

$$\mathcal{L}_f[f_m(\eta)-\chi_mf_{m-1}(\eta)]=\hbar\mathcal{R}_m^f(\eta), \tag{29}$$

$$\mathcal{L}_\theta[\theta_m(\eta)-\chi_m\theta_{m-1}(\eta)]=\hbar\mathcal{R}_m^\theta(\eta), \tag{30}$$

$$\mathcal{L}_\phi[\phi_m(\eta)-\chi_m\phi_{m-1}(\eta)]=\hbar\mathcal{R}_m^\phi(\eta), \tag{31}$$

$f_m(0)=0,f'_m(0)=0,f'_m(\infty)=0$, $\theta_m(0)=0$, $\theta_m(\infty)=0$, and

$$\phi_m(0)=0,\ \phi_m(\infty)=0, \tag{32}$$

$$\begin{aligned}\mathcal{R}_m^f(\eta)=&\\ &f'''_{m-1}+\sum_{k=0}^{m-1}\left[f_{m-1-k}f''_k-2f'_{m-1-k}f'_k\right]+2\lambda^2(1-\chi_m),\end{aligned} \tag{33}$$

$$\begin{aligned}\mathcal{R}_m^\theta(\eta)=&\frac{1}{\Pr}\theta''_{m-1}+\sum_{k=0}^{m-1}(f_{m-1-k}\theta'_k-2f'_{m-1-k}\theta_k)\\ &+\sum_{k=0}^{m-1}(Nb\theta'_{m-1-k}\phi'_k+Nt\theta'_{m-1-k}\theta'_k),\end{aligned} \tag{34}$$

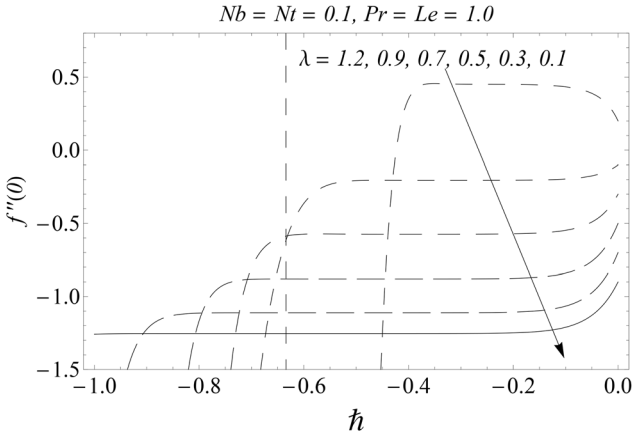

Figure 1. *h*~curves for the function *f*.
doi:10.1371/journal.pone.0061859.g001

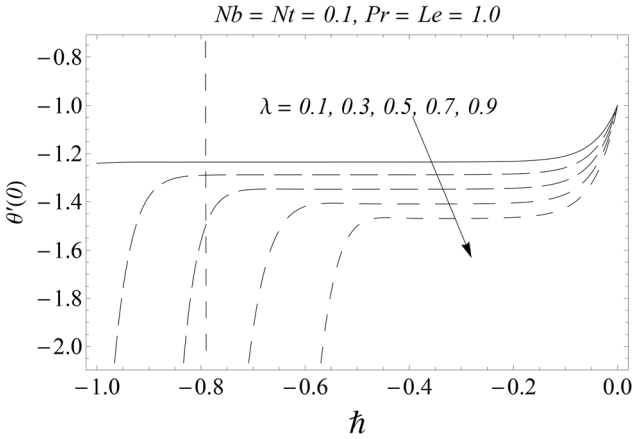

Figure 2. *h* ~curves for the function *θ*.
doi:10.1371/journal.pone.0061859.g002

$$\mathcal{R}_m^{\vartheta}(\eta) = \vartheta''_{m-1} + Le\sum_{k=0}^{m-1}\left(f_{m-1-k}\vartheta'_k - 2f'_{m-1-k}\vartheta_k\right) + \frac{Nt}{Nb}\theta''_{m-1}, \tag{35}$$

$$\chi_m = \begin{cases} 0, & m \le 1, \\ 1, & m > 1. \end{cases} \tag{36}$$

Eqs. (29)–(36) can be easily solved by using the symbolic computation software **Mathematica** for $m = 1,2,3....$

3.1.1 Error analysis and convergence of the homotopy solutions. The auxiliary parameter $\hbar$ in Eqs. (26)–(28) has a key role in the convergence of HAM solutions (see Liao [30]). To select appropriate value of $\hbar$ we have displayed the so-called $\hbar-$curves at 15th-order of approximations for different values of parameter λ in Figs. 1, 2, and 3. Here the valid range of $\hbar$ can be obtained from the flat portion of $\hbar-$curves. The interval of convergence for $\lambda = 1/2$ is $[-0.5, -0.2]$. Further range of $\hbar$ shrinks as we increase the values of λ. To see the accuracy of solutions we define the averaged residuals (see Ref. [36] for details) for the functions f, θ and ϕ as

$$E_{m,1}(\hbar) = \frac{1}{L}\sum_{i=0}^{K}\left[\mathcal{N}_f\left(\sum_{j=0}^{m} f_j(i\Delta x)\right)\right]^2, \tag{37}$$

$$E_{m,2}(\hbar) = \frac{1}{L}\sum_{i=0}^{K}\left[\mathcal{N}_\theta\left(\sum_{j=0}^{m} \theta_j(i\Delta x)\right)\right]^2, \tag{38}$$

$$E_{m,3}(\hbar) = \frac{1}{L}\sum_{i=0}^{K}\left[\mathcal{N}_\phi\left(\sum_{j=0}^{m} \phi_j(i\Delta x)\right)\right]^2, \tag{39}$$

where $\Delta x = 10/L$ and $L = 20$. The averaged residual errors $E_{m,1}$, $E_{m,2}$ and $E_{m,3}$ have been plotted versus $\hbar$ for some fixed values of parameters in Figs. 4, 5, and 6. From these figures we can obtain the best possible value of convergence-control parameter by calculating the minimum values of $E_{m,1}$, $E_{m,2}$ and $E_{m,3}$.

3.2 Numerical method

Eqs. (8)–(10) subject to the boundary conditions (11) have been solved numerically by using the built in function bvp4c of the software MATLAB. This software uses the higher order finite difference code that implements a collocation formula (see Shampine et al. [37] for more details). It will be seen shortly that numerical solutions are in a very good agreement with the homotopy solutions for all the values of the embedding parameters.

Numerical Results and Discussion

The representative results for velocity, temperature and nanoparticles concentration are provided graphically and in tabular form. There is a considerable increase in the velocity with an increase in velocity ratio λ for some fixed values of parameters (see Fig. 7). It is evident from this figure that when $\lambda > 1$, the thickness of the boundary layer decreases with the increase in λ. Here the straining motion near the stagnation region increases so the acceleration of the external stream increases which causes a reduction in the boundary layer thickness and as a consequence

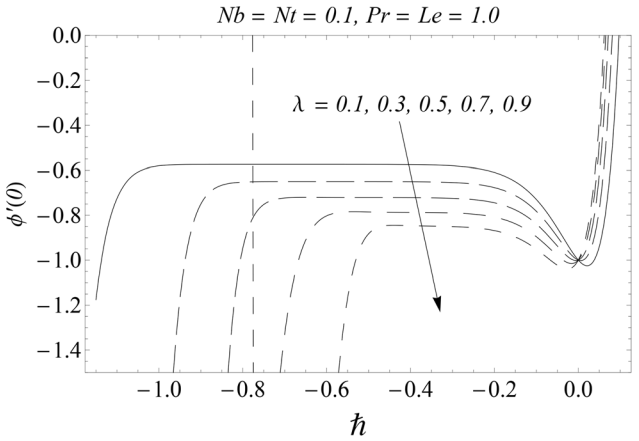

Figure 3. *h* ~curves for the function ϕ.
doi:10.1371/journal.pone.0061859.g003

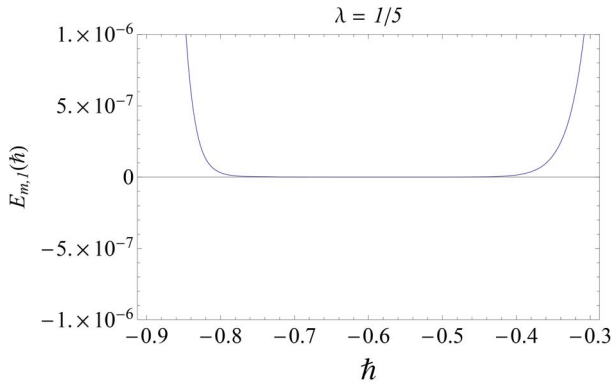

Figure 4. Averaged residual error for the function *f*.
doi:10.1371/journal.pone.0061859.g004

the horizontal velocity increases. On the other hand, when $\lambda<1$, the flow has an inverted boundary layer structure. Here the sheet velocity $U_w(x)$ exceeds the velocity of external stream $U_\infty(x)$. It is also noticed that boundary layer is not formed when $\lambda=1$. Fig. 8 is plotted to perceive the effects of Brownian motion and thermophoresis parameters on the temperature. There is a substantial increase in the temperature and the thermal boundary layer thickness with an increase in *Nb* and *Nt*. The growth in the thermal boundary layer thickness is compensated with smaller rate of heat transfer at the sheet. Fig. 9 portrays the behavior of Prandtl number Pr on the temperature θ. An increase in Pr rapidly shifts the profiles towards the boundary causing a diminution in the thickness of thermal boundary layer. A bigger Prandtl number has a relatively lower thermal diffusivity. Thus an increase in Pr reduces conduction and thereby increases the variation in the thermal characteristics. As expected, the variation in the temperature is more pronounced for smaller values of Pr than its larger values. Fig. 10 depicts the effect of velocity ratio λ on the temperature θ. The temperature and the thermal boundary layer thickness decrease with an increase in λ. Fig. 11 plots the concentration function versus η for different values of the Brownian motion parameter *Nb*. Here unlike the temperature θ, concentration boundary layer reduces as *Nb* increases which thereby enhances the nanoparticles concentration at the sheet. Further we noticed that concentration ϕ is only affected for the values of *Nb* in the range $0<Nb\leq2$. The influence of thermophoresis parameter *Nt* on the concentration boundary layer is noticed in Fig. 12. An abnormal increase in the

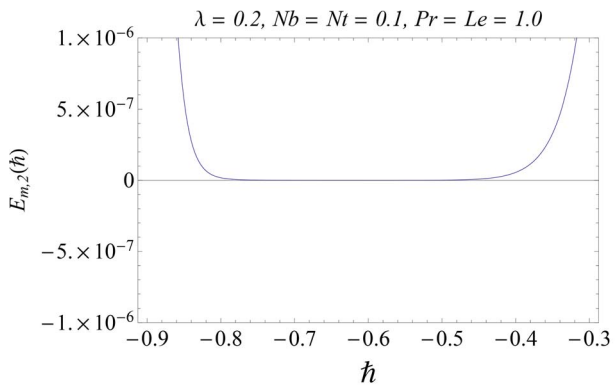

Figure 5. Averaged residual error for the function *θ*.
doi:10.1371/journal.pone.0061859.g005

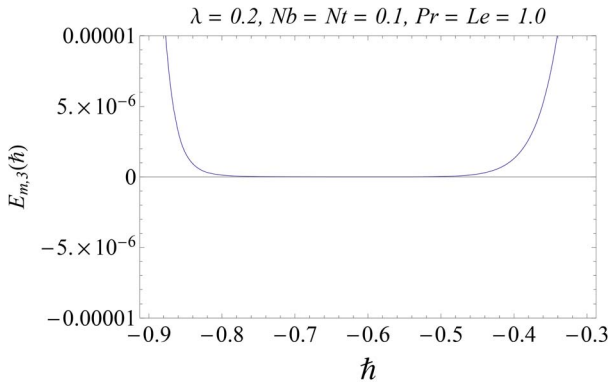

Figure 6. Averaged residual error for the function ϕ.
doi:10.1371/journal.pone.0061859.g006

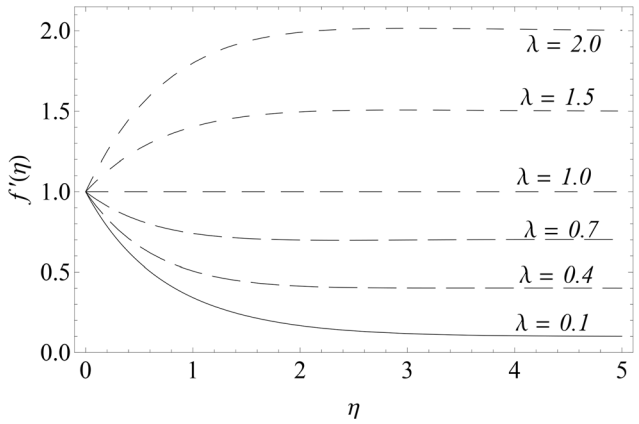

Figure 7. Influence of λ on $f'(\eta)$.
doi:10.1371/journal.pone.0061859.g007

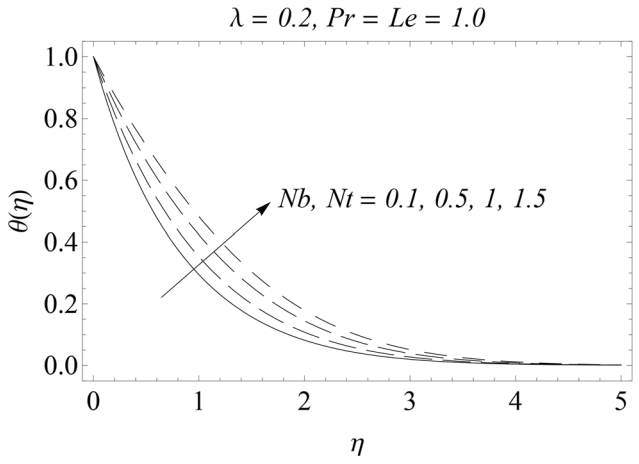

Figure 8. Influence of Nb and Nt on $\theta(\eta)$.
doi:10.1371/journal.pone.0061859.g008

concentration ϕ is found for a weaker Brownian motion ($Nb=0.2$). In fact an over shoot in the concentration function occurs as we gradually increase *Nt*. On the other hand, when the effect of Brownian motion is increased i.e *Nb* changes from 0.2 to 1, there is a little increase in the concentration ϕ with an increase in *Nt*. This outcome is attributed to the fact that an increase in *Nt*

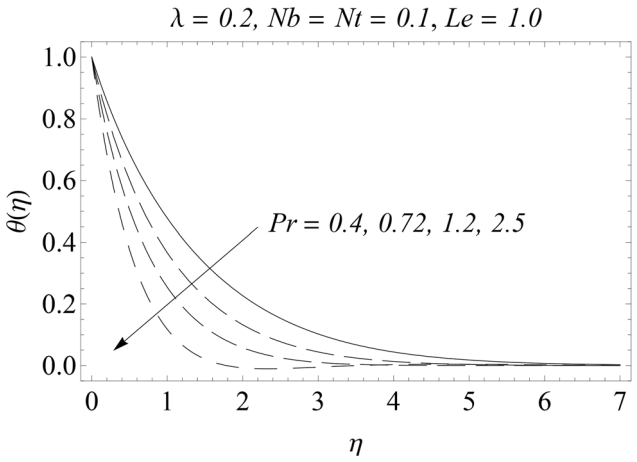

Figure 9. Influence of Pr on $\theta(\eta)$.
doi:10.1371/journal.pone.0061859.g009

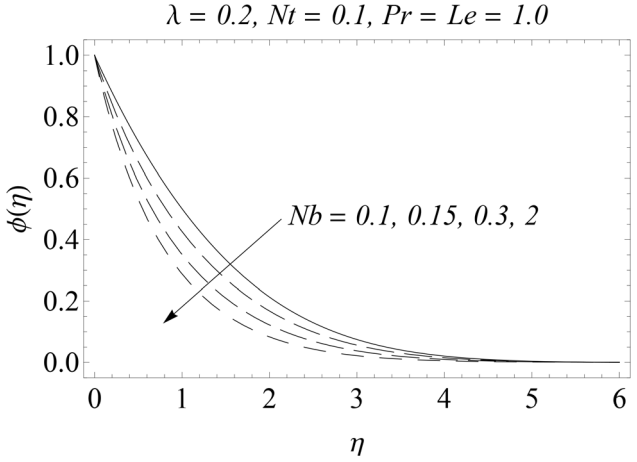

Figure 11. Influence of Nb on $\phi(\eta)$.
doi:10.1371/journal.pone.0061859.g011

appreciably enhances the mass flux due to temperature gradient which in turn rises the nanoparticles concentration. The behavior of Lewis number *Le* on the concentration field ϕ is presented in Fig. 13. As *Le* gradually increases, this corresponds to a weaker molecular diffusivity and thinner concentration boundary layer. In accordance with [27] the variation in ϕ with *Le* is prominent neat the stretching wall. Fig. 14 shows that the influence of λ on the nanoparticles concentration ϕ is virtually similar to that accounted for the temperature θ.

Reduced Nusselt number $Nur = (-\theta'(0))$ for different values of *Nb* is plotted versus *Nt* in the Fig. 15. It is observed that for a weaker thermophoretic effect, there is a significant decrease in the rate of heat transfer at the sheet with an increase in *Nb*. However when the strength of thermophoretic is increased i.e *Nb* changes from 0.1 to 2 the absolute decrease in *Nur* with an increase in *Nt* is negligible. This reduction actually occurs due to the excessive movement of nanoparticles from the stretching wall to the quiescent fluid. Fig. 16 shows the simultaneous effects of *Nb* and *Nt* on the reduced sherwood number *Shr*. There is a slight increase in *Shr* with an increase in *Nb* when the thermophoretic effect is weak. However this increase is significant when the thermophoretic effect intensifies. The variations of *Nur* and *Shr* with the velocity ratio λ is sketched in the Figs. 17 and 18. The

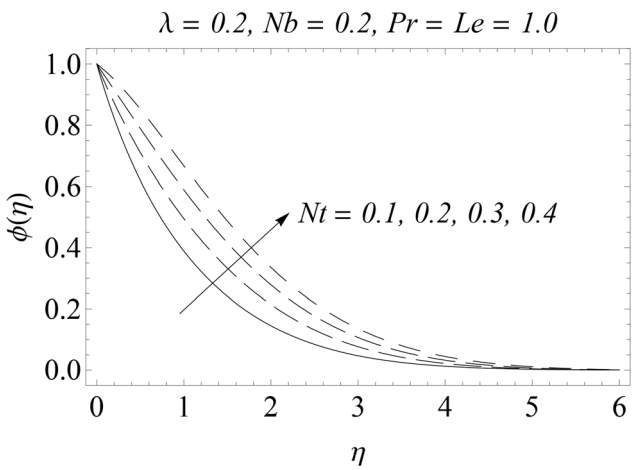

Figure 12. Influence of Nt on $\phi(\eta)$.
doi:10.1371/journal.pone.0061859.g012

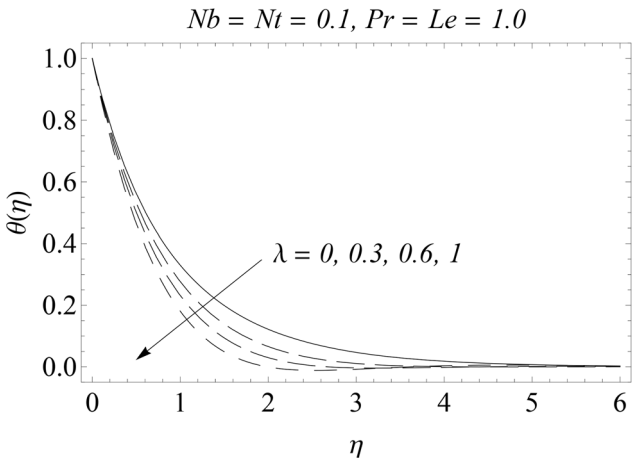

Figure 10. Influence of λ on $\theta(\eta)$.
doi:10.1371/journal.pone.0061859.g010

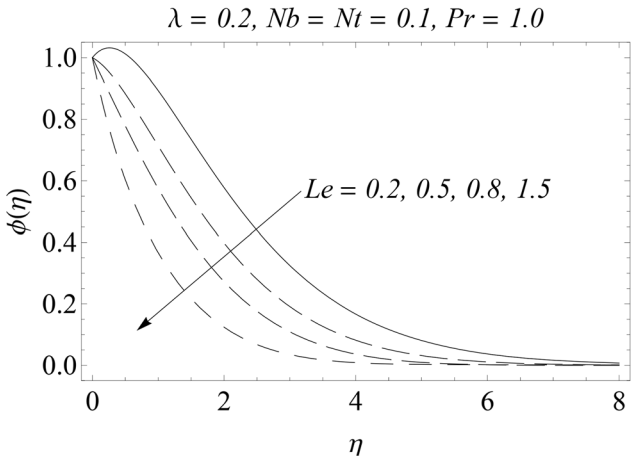

Figure 13. Influence of Le on $\phi(\eta)$.
doi:10.1371/journal.pone.0061859.g013

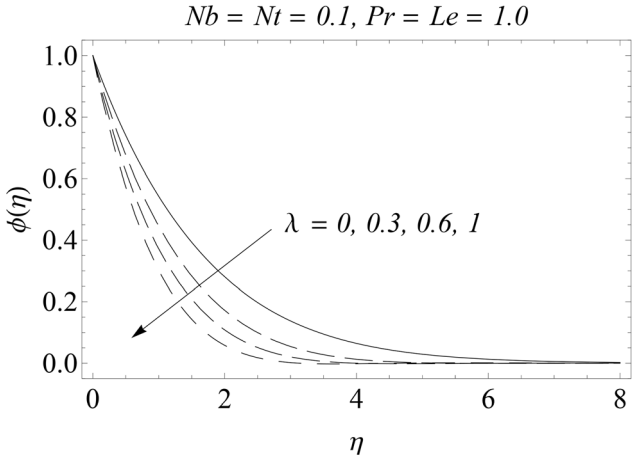

Figure 14. Influence of λ on $\phi(\eta)$.
doi:10.1371/journal.pone.0061859.g014

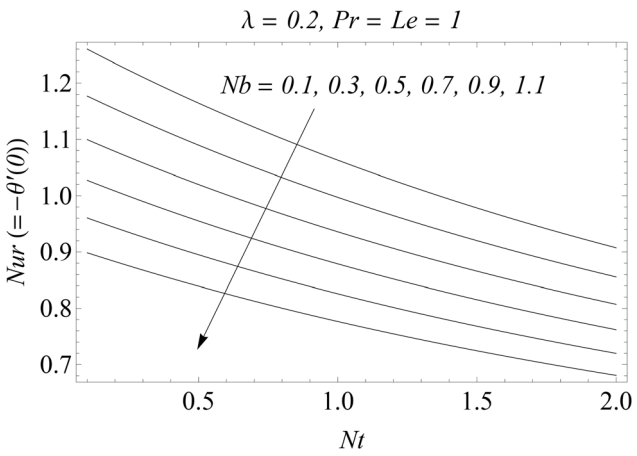

Figure 15. Influence of *Nb* and *Nt* on *Nur*.
doi:10.1371/journal.pone.0061859.g015

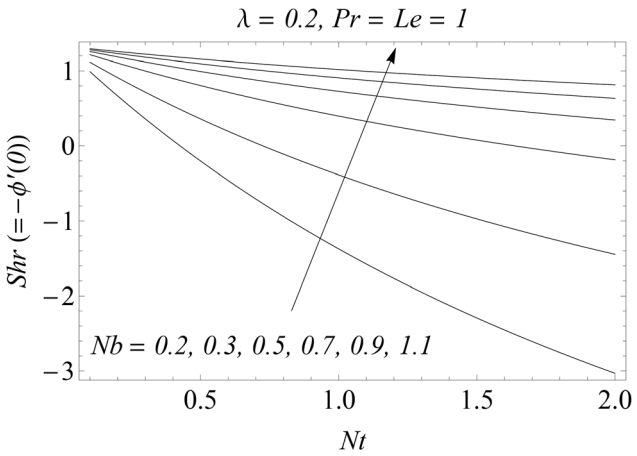

Figure 16. Influence of *Nb* and *Nt* on *Shr*.
doi:10.1371/journal.pone.0061859.g016

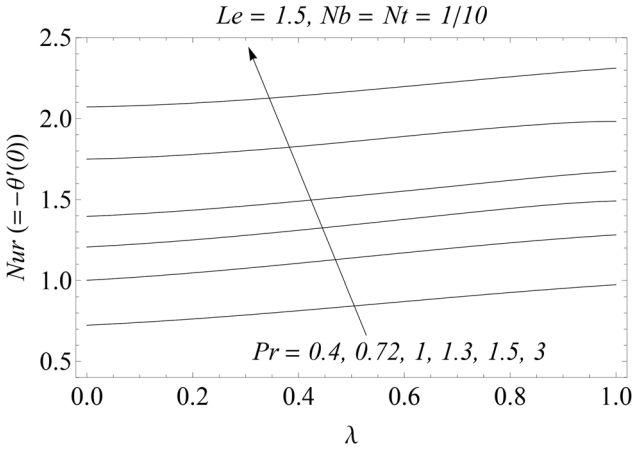

Figure 17. Influence of λ and *Pr* on *Nur*.
doi:10.1371/journal.pone.0061859.g017

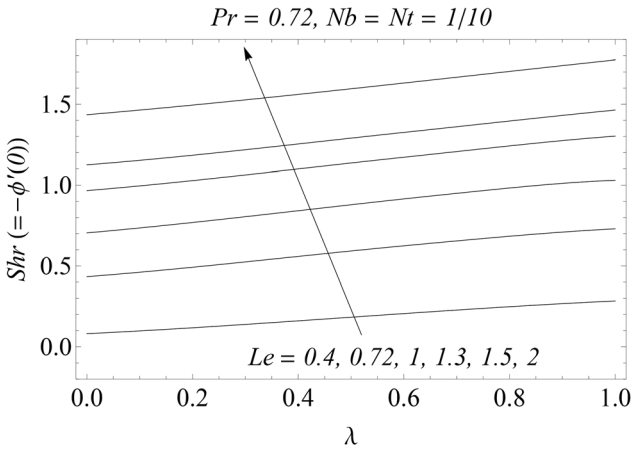

Figure 18. Influence of λ and Le on *Shr*.
doi:10.1371/journal.pone.0061859.g018

Table 1. Numerical values of skin friction coefficient $f''(0)$ for different values of velocity ratio parameter λ.

λ	$\sqrt{2\mathrm{Re}}C_f = f''(0)$	
	HAM	**Numerical**
0	−1.281809	−1.281810
0:1	−1.253580	−1.253580
0:2	−1.195118	−1.195120
0:5	−0.879833	−0.879835
0:8	−0.397767	−0.397771
1:2	0.451568	0.451571

doi:10.1371/journal.pone.0061859.t001

Table 2. Numerical values of Nur and Shr for different values of Pr and Le when $\lambda = 0.2$, $Nb = Nt = 0.1$ and $h = -0.7$.

Pr	Le	$Nur = -\theta'(0)$		$Shr = -\phi'(0)$	
		HAM	**Numerical**	**HAM**	**Numerical**
0.4	1	0.74994	0.74994	0.97397	0.97399
0.7		1.03426	1.03430	0.77875	0.77875
1.0		1.26024	1.26020	0.61269	0.61269
1.2		1.39072	1.39070	0.51328	0.51328
1.0	0.4	1.28094	1.28090	−0:11720	−0.11720
	0.7	1.26862	1.26860	0.29218	0.29218
	1.2	1.25588	1.25590	0.79694	0.76965
	1.5	1.25052	1.25050	1.04315	1.04320

doi:10.1371/journal.pone.0061859.t002

dimensionless heat and mass transfer rates at the sheet increase when λ is increased. In Table 1 the dimensionless velocity gradient on the sheet is approximated for various values of λ. We observed that skin friction coefficient is reduced by assuming sufficiently large values of λ. The numerical values of Nur and Shr corresponding to different values of Pr and Le have been given in Table 2. It is clear from this table that numerical and analytical solutions are in a very good agreement. We noticed earlier that increase in Pr and Le reduce the thermal boundary layer thickness and curves become steeper. The reduced Nusselt and Sherwood numbers, being proportional to the corresponding initial slopes, increase with an increase in Pr and Le respectively.

Conclusions

Flow of nanofluid in the region of stagnation-point towards an exponentially stretching sheet is studied. The developed mathematical problems have been solved for series solutions. A very good averaged residual error of about 10^{-10} is achieved at only 15th-order of approximations in nearly all the cases. The numerical solutions are computed by the built-in solver bvp4c of the software MATLAB. Analytic and numerical solutions are found in excellent agreement for all the values of embedding parameters. It is observed that the velocity ratio λ has a dual behavior on the momentum boundary layer. An increase in the strengths of Brownian motion and thermophoretic effects causes an appreciable increase in the temperature and the thermal boundary layer thickness. The current analysis for the case of regular fluid, which is not yet reported can be obtained by setting $Nb = Nt = 0$.

Author Contributions

Analyzed the data: MM TH MAF. Contributed reagents/materials/analysis tools: MM TH MAF AA. Wrote the paper: MM TH.

References

1. Blasius H (1908) Grenzschichten in Flussigkeiten mit Kleiner Reibung. Z Angew Math Phys 56: 1–37.
2. Sakiadis BC (1961) Boundary-layer behaviour on continuous solid surfaces. I. Boundary-layer equations for two-dimensional and axisymmetric flow. AIChE J 7: 26–28.
3. Crane LJ (1970) Flow past a stretching plate. Z Angew Math Phys 21: 645–647.
4. Rajagopal KR, Na TY, Gupta AS (1984) Flow of a viscoelastic fluid over a stretching sheet. Rheol Acta 23: 213–215.
5. Mahapatra TR, Gupta AS (2004) Stagnation-point flow of a viscoelastic fluid towards a stretching surface. Int J Nonlinear Mech 39: 811–820.
6. Cortell R (2007) MHD flow and mass transfer of an electrically conducting fluid of second grade in a porous mediumover a stretching sheet with chemically reactive species. Chem Eng Process 46: 721–728.
7. Bachok N, Ishak A, Pop I (2010) Melting heat transfer in boundary layer stagnationpoint.flow towards a stretching/shrinking sheet. Phys Lett A 374: 4075–4079.
8. Abbasbandy S, Ghehsareh HR (2012) Solutions of the magnetohydrodynamic .ow over a nonlinear stretching sheet and nano boundary layers over stretching surfaces. Int J Num Meth Fluids 70: 1324–1340.
9. Fang T, Zhang J, Zhong Y (2012) Boundary layer flow over a stretching sheet with variable thickness. Appl Math Comput 218: 7241–7252.
10. Hayat T, Mustafa M, Hendi AA (2011) Time-dependent three-dimensional flow and mass transfer of elastico-viscous .uid over unsteady stretching sheet. Appl Math Mech-Engl Ed 32: 167–178.
11. Mustafa M, Hayat T, Hendi AA (2012) Influence of melting heat transfer in the stagnation-point flow of a Jeffrey fluid in the presence of viscous dissipation. ASME-J Appl Mech 79: 021504 (1–5).
12. Mustafa M, Hayat T, Obaidat S (2012) Stagnation-point flow and heat transfer of a Casson fluid towards a stretching sheet. Z Naturforsch 67a: 70–76.
13. Magyari E, Keller B (1999) Heat and mass transfer in the boundary layers on an expo-nentially stretching continuous surface. J Phys D Appl Phys 32: 577–585.
14. Elbashbeshy EMA (2001) Heat transfer over an exponentially stretching continuous surface with suction. Arch Mech 53: 643–651.
15. Khan S, Sanjayanand K (2005) Viscoelastic boundary layer flow and heat transfer over an exponential stretching sheet. Int J Heat Mass Transfer 48: 1534–1542.
16. Sajid M, Hayat T (2008) In.uence of thermal radiation on the boundary layer flow due to an exponentially stretching sheet. Int Comm Heat Mass Transfer 35: 347–356.
17. Nadeem S, Hayat T, Malik MY, Rajput SA (2010) Thermal radiation effects on the flow by an exponentially stretching surface: a series solution. Z Naturforsch 65a: 495–503.
18. Daungthongsuk W, Wongwises S (2007) A critical review of convective heat transfer nanofluids. Renew Sust Eng Rev 11: 797–817.
19. Wang XQ, Mujumdar AS (2008) A review on nanofluids–Part I: theoretical and nu-merical investigations. Brazilian J Chem Eng 25: 613–630.
20. Wang XQ, Mujumdar AS (2008) A review on nanofluids–Part II: experiments and applications. Brazilian J Chem Eng 25: 631–648.
21. Kakaç S, Pramuanjaroenkij A (2009) Review of convective heat transfer enhancement with nanofluids. Int J Heat Mass Transfer 52: 3187–3196.
22. Kuznetsov AV, Nield DA (2010) Natural convective boundary-layer flow of a nanofluid past a vertical plate. Int J Thermal Sci 49: 243–247.
23. Nield DA, Kuznetsov AV (2009) The Cheng–Minkowycz problem for natural convective boundary-layer flow in a porous medium saturated by a nanofluid. Int J Heat Mass Transfer 52: 5792–5795.
24. Bachok N, Ishak A, Pop I (2010) Boundary-layer flow of nanofluids over a moving surface in a flowing fluid. Int J Therm Sci 49: 1663–1668.
25. Khan WA, Pop I (2010) Boundary-layer flow of a nanofluid past a stretching sheet. Int J Heat Mass Transfer 53: 2477–2483.
26. Rana P, Bhargava R (2012) Flow and heat transfer of a nanofluid over a nonlinearly stretching sheet: A numerical study. Comm Nonlinear Sci Num Simul 17: 212–226.
27. Makinde OD, Aziz A (2011) Boundary layer flow of a nanofluid past a stretching sheet with a convective boundary condition. Int J Therm Sci 50: 1326–1332.
28. Yacob NA, Ishak A, Nazar R, Pop I (2011) Falkner.Skan problem for a static and moving wedge with prescribed surface heat flux in a nanofluid. Int Comm Heat Mass Transfer 38: 149–153.

29. Mustafa M, Hayat T, Pop I, Asghar S, Obaidat S (2011) Stagnation-point flow of a nanofluid towards a stretching sheet. Int J Heat Mass Transfer 54: 5588–5594.
30. Liao SJ (2009) Notes on the homotopy analysis method: Some definitions and theorems. Comm Non-linear Sci Num Simul 14: 983–997.
31. Liao SJ (2010) On the relationship between the homotopy analysis method and Euler transform. Comm Nonlinear Sci Numer Simul 15: 1421–1431:
32. Abbasbandy S, Shirzadi A (2011) A new application of the homotopy analysis method: Solving the Sturm–Liouville problems. Comm Nonlinear Sci Num Simul 16: 112–126.
33. Mustafa M, Hayat T, Obaidat S (2012) On heat and mass transfer in the unsteady squeezing flow between parallel plates. Mecc 47: 1581–1589.
34. Hayat T, Mustafa M, Asghar S (2010) Unsteady flow with heat and mass transfer of a third grade fluid over a stretching surface in the presence of chemical reaction. Non-Linear Anal RWA 11: 3186–3197.
35. Rashidi MM, Pour SAM, Abbasbandy S (2011) Analytic approximate solutions for heat transfer of a micropolar fluid through a porous medium with radiation. Comm Nonlinear Sci Num Simul 16: 1874–1889.
36. Liao S (2010) An optimal homotopy-analysis approach for strongly nonlinear differential equations. Comm Nonlinear Sci Num Simul 15: 2003–2016.
37. Shampine LF, Kierzenka J, Reichelt MW (2003) Solving boundary value problems for ordinary differential equations in MATLAB with bvp4cTutorial Notes. Available at http://www.mathworks.com/bvp_tutorial.